Research Article | Vol. 25, No. 11 | 29 May 2017 | OPTICS EXPRESS 12295
Optics EXPRESS

Hybrid plasmonic waveguides formed by metal coating of dielectric ridges

VLADIMIR A. ZENIN,[1,*] SAJID CHOUDHURY,[2] SOHAM SAHA,[2] VLADIMIR M. SHALAEV,[2] ALEXANDRA BOLTASSEVA,[2] AND SERGEY I. BOZHEVOLNYI[1]

[1]*Centre for Nano Optics, University of Southern Denmark, Campusvej 55, DK-5230 Odense, Denmark*
[2]*School of Electrical and Computer Engineering and Birck Nanotechnology Center, Purdue University, West Lafayette IN, 47907, USA*
[*]*zenin@mci.sdu.dk*

Abstract: Bound hybrid plasmon-polariton modes supported by waveguides, which are formed by gold coating of ridges etched into a silica substrate, are analyzed using numerical simulations and investigated experimentally using near-field microscopy at telecom wavelengths (1425-1625 nm). Drastic modifications of the fundamental mode profile along with changes in the mode confinement and propagation loss are found when varying the ridge height. The main mode characteristics (effective mode index, propagation length, and mode profile) are determined from the experimental amplitude- and phase-resolved near-field images and compared with the simulations. The possibility of strongly influencing the mode properties along with subwavelength confinement found simultaneously with relatively long propagation can further be exploited in mode shaping and sensing applications.

© 2017 Optical Society of America

OCIS codes: (230.7370) Waveguides; (180.4243) Near-field microscopy; (240.6680) Surface plasmons; (250.5403) Plasmonics.

References and links

1. H. Raether, *Surface Plasmons on Smooth and Rough Surfaces and on Gratings* (Springer, 1988).
2. D. K. Gramotnev and S. I. Bozhevolnyi, "Nanofocusing of electromagnetic radiation," Nat. Photonics **8**, 13–22 (2014).
3. V. A. Zenin, A. Andryieuski, R. Malureanu, I. P. Radko, V. S. Volkov, D. K. Gramotnev, A. V. Lavrinenko, and S. I. Bozhevolnyi, "Boosting local field enhancement by on-chip nanofocusing and impedance-matched plasmonic antennas," Nano Lett. **15**(12), 8148–8154 (2015).
4. R. F. Oulton, G. Bartal, D. F. P. Pile, and X. Zhang, "Confinement and propagation characteristics of subwavelength plasmonic modes," New J. Phys. **10**(10), 105018 (2008).
5. A. A. Vyshnevyy and D. Yu. Fedyanin, "Spontaneous emission and fundamental limitations on the signal-to-noise ratio in deep-subwavelength plasmonic waveguide structures with gain," Phys. Rev. Appl. **6**(6), 064024 (2016).
6. S. Lal, S. Link, and N. J. Halas, "Nano-optics from sensing to waveguiding," Nat. Photonics **1**(11), 641–648 (2007).
7. C. Haffner, W. Heni, Y. Fedoryshyn, J. Niegemann, A. Melikyan, D. L. Elder, B. Baeuerle, Y. Salamin, A. Josten, U. Koch, C. Hoessbacher, F. Ducry, L. Juchli, A. Emboras, D. Hillerkuss, M. Kohl, L. R. Dalton, C. Hafner, and J. Leuthold, "All-plasmonic machâĂŞzehnder modulator enabling optical high-speed communication at the microscale," Nat. Photonics **9**(8), 525–528 (2015).
8. S. J. P. Kress, F. V. Antolinez, P. Richner, S. V. Jayanti, D. K. Kim, F. Prins, A. Riedinger, M. P. C. Fischer, S. Meyer, K. M. McPeak, D. Poulikakos, and D. J. Norris, "Wedge waveguides and resonators for quantum plasmonics," Nano Lett. **15**(9), 6267–6275 (2015).
9. S. I. Bozhevolnyi and J. B. Khurgin, "Fundamental limitations in spontaneous emission rate of single-photon sources," Optica **3**(12), 1418–1421 (2016).
10. J. S. Clausen, E. Højlund-Nielsen, A. B. Christiansen, S. Yazdi, M. Grajower, H. Taha, U. Levy, A. Kristensen, and N. A. Mortensen, "Plasmonic metasurfaces for coloration of plastic consumer products," Nano Lett. **14**(8), 4499–4504 (2014).
11. T. Holmgaard and S. I. Bozhevolnyi, "Theoretical analysis of dielectric-loaded surface plasmon-polariton waveguides," Phys. Rev. B **75**(24), 245405 (2007).
12. T. Holmgaard, S. I. Bozhevolnyi, L. Markey, A. Dereux, A. V. Krasavin, P. Bolger, and A.V. Zayats, "Efficient excitation of dielectric-loaded surface plasmon-polariton waveguide modes at telecommunication wavelengths," Phys. Rev. B **78**(16), 165431 (2008).
13. E. Palik and G. Ghosh, *Handbook of Optical Constants of Solids II* (Academic Press, 1991).

#286076 https://doi.org/10.1364/OE.25.012295
Journal © 2017 Received 2 Feb 2017; accepted 5 May 2017; published 17 May 2017

Optics EXPRESS

14. A. Andryieuski, V. A. Zenin, R. Malureanu, V. S. Volkov, S. I. Bozhevolnyi, and A. V. Lavrinenko, "Direct characterization of plasmonic slot waveguides and nanocouplers," Nano Lett. **14**(7), 3925–3929 (2014).
15. M. Schnell, A. Garcia-Etxarri, A. J. Huber, K. B. Crozier, A. Borisov, J. Aizpurua, and R. Hillenbrand, "Amplitude- and phase-resolved near-field mapping of infrared antenna modes by transmission-mode scattering-type near-field microscopy," J. Phys. Chem. C **114**(16), 7341–7345 (2010).
16. V. A. Zenin, A. Pors, Z. Han, R. L. Eriksen, V. S. Volkov, and S. I. Bozhevolnyi, "Nanofocusing in circular sector-like nanoantennas," Opt. Express **22**(9), 10341âĂŞ10350 (2014).
17. V. A. Zenin, R. Malureanu, I. P. Radko, A. V. Lavrinenko, and S. I. Bozhevolnyi, "Near-field characterization of bound plasmonic modes in metal strip waveguides," Opt. Express **24**(5), 4582–4590 (2016).
18. N. Ocelic, A. Huber, and R. Hillenbrand, "Pseudoheterodyne detection for background-free near-field spectroscopy," Appl. Phys. Lett. **89**, 101124 (2006).
19. A. Boltasseva, V. S. Volkov, R. B. Nielsen, E. Moreno, S. G. Rodrigo, and S. I. Bozhevolnyi, "Triangular metal wedges for subwavelength plasmon-polariton guiding at telecom wavelengths," Opt. Express **16**(8), 5252–5260 (2008).
20. R. B. Nielsen, I. Fernandez-Cuesta, A. Boltasseva, V. S. Volkov, S. I. Bozhevolnyi, A. Klukowska, and A. Kristensen, "Channel plasmon polariton propagation in nanoimprinted V-groove waveguides," Opt. Lett. **33**(23), 2800–2802 (2008).

1. Introduction

Surface plasmon polaritons (SPPs) are well known for the ability to confine electromagnetic field to a metal-dielectric interface [1], allowing for nanofocusing with tremendous field enhancement [2, 3]. However, a long-lasting dream of replacing slow electronic circuits with fast and still small plasmonic components appeared to be fundamentally insoluble due to the omnipresent trade-off between mode confinement and propagation losses [4]. Even if propagation losses are compensated by the incorporation of a gain medium in the waveguide, the noise and spontaneous emission casts doubt on its practical use [5]. Nevertheless, plasmonics found its practical application in a variety of sensors [6] and active components [7]. Also recently it was shown that plasmonic cavities are advantageous for quantum optics due to their high Purcell factors [8]. Moreover, it appears that plasmonic waveguides have significant advantages over photonic (dielectric-based) waveguides with respect to the achievable levels of enhancement in single-photon emission rates [9]. Thus, it is not only the mode confinement and propagation length which matter, but other factors such as mode shaping possibilities, fabrication complexity and the availability of the mode field to the external quantum emitters need to be considered upon choosing the best waveguide design for a particular application. Here, we present a novel hybrid waveguide design formed by metal-deposition onto a dielectric substrate with a ridge. Its design was inspired by similarly produced metal disc-on-hole plasmonic antennas [10], which share similar features. The field of the mode is partially emerged from the ridge sides into the air, making it available for coupling with external quantum emitters. The waveguide design is comparable in simplicity to the dielectric-loaded SPP waveguides, where a dielectric ridge is placed on a flat metal film [11, 12]. However, our hybrid waveguide design offers additional features, such as the possibility of drastically changing the fundamental mode profile and extending the mode field outside the ridges along with achieving relatively long propagation for strongly confined modes. These features make this plasmonic waveguide configuration interesting for mode shaping (for example, for nanofocusing [2, 3]) and sensing applications as well as for enhancing single-photon emission rates in quantum plasmonics [9].

In the following, we present the results of detailed numerical and experimental investigations of the mode properties (effective mode index, propagation length, and mode profile) when it is guided along a hybrid waveguide with a gold film deposited on a silica substrate with a ridge at the telecom wavelengths near 1500 nm. First waveguiding properties are studied numerically with a finite element method (FEM) implemented in COMSOL software. Then waveguides, fabricated with a metal film thickness of 70 nm, ridge height of 200 nm, and two ridge widths of 200 and 300 nm, are investigated in amplitude- and phase-resolved scattering-type scanning near-field optical microscope (SNOM). The recorded complex-valued near-field maps are then

Optics EXPRESS

fitted in MATLAB in order to determine the effective mode index, propagation length, and mode profile. Finally, we compare the numerical and experimental results and discuss further developments.

2. Numerical investigation of dispersion properties

The investigated structure consists of a silica ridge of width w and height h, coated on the top with a gold layer of thickness t [inset in Fig. 1(a)]. The edges of the top gold strip were rounded with radius $r = 10$ nm in order to better represent real fabricated structures. The default parameters were $w = 300$ nm, $t = 70$ nm, $\lambda = 1500$ nm, and should be assumed everywhere unless otherwise stated. The value for the permittivity of gold was taken from [13] and it is $\varepsilon_{\text{gold}} = -90 + 10.1i$ at $\lambda = 1500$ nm, while the refractive index of silica was assumed to be 1.4446. We studied the fundamental mode in which electric field inside the ridge is mainly normal to the substrate [Figs. 1(b)-(d)]. The dispersion properties of the mode are presented in Fig. 1(a) in terms of the propagation length vs. the effective mode index, with the ridge height being varied. As intuitively expected, the decrease of ridge height, wavelength, or metal thickness leads to the increase in the effective mode index and the decrease of the propagation length. The change of the ridge width might either increase or decrease the mode confinement. However, the corresponding dispersion curves do not differ significantly, which illustrates the above-mentioned trade-off between confinement and propagation losses.

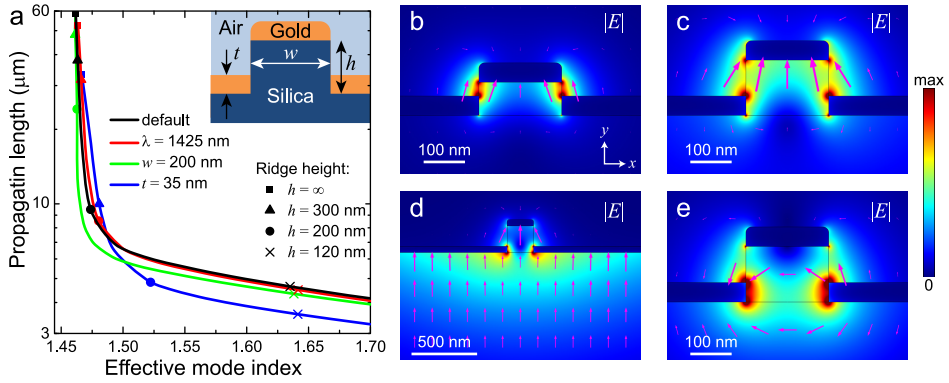

Fig. 1. (a) Propagation length as a function of effective mode index for default parameters ($t = 70$ nm, $\lambda = 1500$ nm, $w = 300$ nm; black) and modified parameters: $\lambda = 1425$ nm (red), $w = 300$ nm (green), and $t = 35$ nm (blue), calculated for varied ridge height. Selected values of ridge height are shown with squares ($h = \infty$), triangles ($h = 300$ nm), circles ($h = 200$ nm), and crosses ($h = 120$ nm). Inset shows an illustration of the studied hybrid waveguide design. (b-e) Electric-field amplitude mode profiles for ridge height of: (b) 120 nm, (c, e) 200 nm, and (d) 300 nm, respectively. Profile (e) shows a second mode supported by the waveguide with the opposite field symmetry. The magenta arrows schematically depict the direction of the transverse electric field. Black lines represent the material boundaries.

As for the mode profiles, at small ridge height, the field is strongly confined between gold edges along side walls of the ridge [Fig. 1(b)], causing low propagation length. For taller ridges, the mode field spreads more inside the ridge [Fig. 1(c)]. Finally, at large ridge height, the effective mode index becomes quite low and close to the refractive index of the substrate, and the mode is no more confined to the ridge [Fig. 1(d)], but instead approaches the planar bound SPP mode of the gold film on silica in terms of the mode profile and dispersion [squares in Fig. 1(a)]. Therefore, for experimental investigations, we chose an intermediate ridge height of 200 nm, which features both strong confinement and relatively long propagation length. It is worth men-

Optics EXPRESS

tioning that such waveguide also supports another mode of opposite field-symmetry when the electric field inside the ridge is mainly orthogonal and along x-axis [Fig. 1(e)]. Such mode is quite similar to the usual plasmonic slot mode [14], therefore we decided to not investigate it further.

3. Experimental investigation

3.1. Fabrication process

In order to fabricate the waveguide prototypes, we etched fused silica substrate through a mask. Figure 2 shows the fabrication steps. A 500-μm-thick double-side polished fused silica wafer is diced into 1.5 cm by 1.5 cm pieces. A 100 nm layer of Cr is deposited onto the substrate as a hard mask, using an electron-beam (E-beam) evaporator. 6% Hydrogen silsesquioxane (HSQ) solution is spin-coated onto the substrate at 1000 rpm (resist thickness of 190 nm). The resist is post-baked at 80°C for 4 minutes. The patterns are exposed using E-beam lithography with a dose of 1600 μC/cm^2 (Vistec VB6 machine). Immediately after exposure, the sample is developed in 25% Tetramethyl ammonium hydroxide (TMAH) solution for 30 seconds, rinsed with DI water for 1 minute and blow-dried with a N_2 gun. After development, the sample is post-baked at 105°C for 3 minutes. The Cr layer is etched using reactive ion etcher (RIE) with a mixture of Cl_2 and O_2 (Cl_2 flow rate = 26 sccm, O_2 flow rate = 4 sccm, RF source bias power = 400 W, forward bias power = 20 W, pressure = 1 Pa, etch rate = 20 nm/min). Using the chromium layer as a mask, the SiO_2 is now etched with RIE (CHF_3 flow rate= 45 sccm, O_2 flow rate = 4 sccm, RF source bias power = 500 W, forward bias power = 100 W, pressure = 0.5 Pa, etch rate = 100 nm/min). The CHF_3 etch removes part of the developed HSQ resist and etches the SiO_2 substrate. The remaining Cr-masking layer is removed by sonicating it in CR-7 chrome etchant for 10 minutes. A Ti adhesion layer of 10 nm and 60 nm of gold is subsequently deposited by E-beam evaporation at 2 Å/s. Upon fabrication trials, we found the tendency of gold to form a meniscus with silica ridge walls, which, according to our simulations, results in the decreased propagation length. Moreover, if the top and bottom gold layers are connected, the considered mode is no longer supported by the waveguide. In order to avoid it, one should use a high ratio of the ridge height to the metal thickness (in our case it was 3:1). Another option is to slightly undercut the ridge, which we used by optimizing the pressure of the SiO_2 etch.

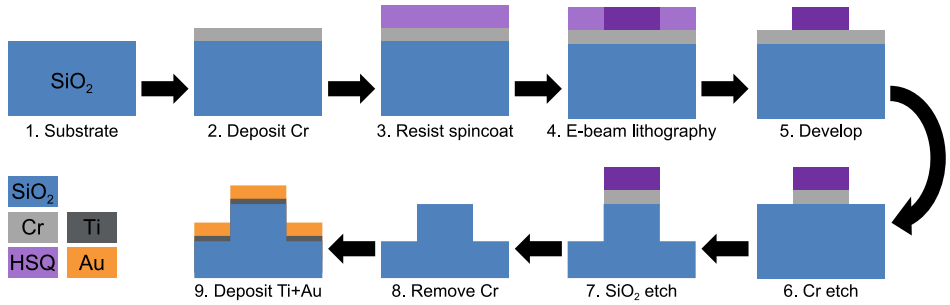

Fig. 2. Fabrication steps.

3.2. Experimental arrangement

The fabricated 35-μm-long waveguides of height ~200 nm and width 200 and 300 nm were terminated with a side-rib grating, used for the excitation with normal illumination (Fig. 3). The grating had a period of ~1 μm, while its shape and size were not optimized for best performance. The structures were experimentally investigated using a scattering-type SNOM, based

Optics EXPRESS

on an atomic force microscope (AFM). The radiation from a tunable telecom laser was incident normally on the sample from below (transmission mode [3, 14–17]), and a platinum-coated AFM Si probe, operating in a tapping mode at a frequency of $\Omega \approx 250$ kHz, was scattering the near-field of the sample, collected with a top parabolic mirror [Fig. 3(a)]. The lower parabolic mirror was moving synchronously with the sample in the xz-plane during the scan in order to maintain the excitation alignment. The signal was detected and demodulated at the third harmonic (3Ω) to filter the near-field contribution from the background. In order to resolve both the amplitude and the phase of the near-field, we used a reference beam and interferometric pseudoheterodyne detection [18].

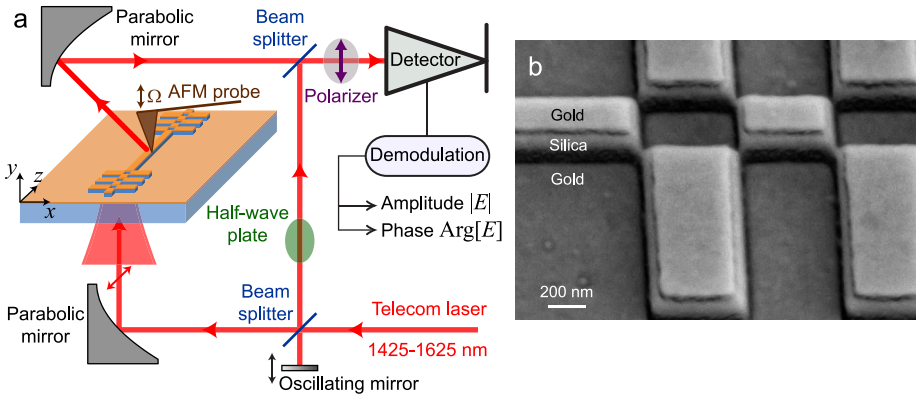

Fig. 3. (a) Schematic layout of the background-free amplitude- and phase-resolved scattering-type SNOM. (b) SEM image of the waveguide terminated with the grating, produced with primary and back-scattered electron detectors at 52° tilt. Dark region represents silica.

3.3. Near-field maps

The near-field maps of the 8-μm-long part of the waveguides are shown in Figure 4. The phase maps clearly demonstrate mode propagation along the waveguide. The amplitude maps show decay along the waveguide, which illustrates moderate propagation losses. Also one can notice pronounced fringes of the length ~2-3 μm, which is a sign of a multimode behavior. Thus a direct measurement of the mode propagation constant is not possible from near-field maps. However, it can be found by Fourier analysis and subsequent fitting of the near-field maps with a discrete number of co-propagating modes, similarly to our previous works [3, 14, 17].

3.4. Fitting of near-field maps

First, we analyzed the recorded complex-valued near-field maps with one-dimensional Fourier transformation (FT) along the propagation direction (i.e., the z-axis is transformed into k_z axis). On Fourier amplitude maps, it can be seen that there are 2 co-propagating modes: one with an effective mode index around $n_{\text{eff}} \approx 1.5$ (which is a fundamental mode we are looking for) and another with $n_{\text{eff}} \approx 1$ (low left image in Fig. 5). The second mode is most probably leaky SPP running on top of the gold. Also one can notice a dim sign of the reflected second mode, which altogether produce a complex interference pattern on near-field maps (Fig. 4).

In order to accurately determine the dispersion properties of the mode, we applied numerical fitting of the recorded near-field maps with a superposition of two modes, similar to as was done in [3, 14, 17]. It can be seen that the assumption of two modes describes well the complex near-field pattern (Fig. 5). A small but non-zero residual field can be explained by the presence of other waveguiding modes or any radiation, which is not along the waveguide. The amplitude

Optics EXPRESS

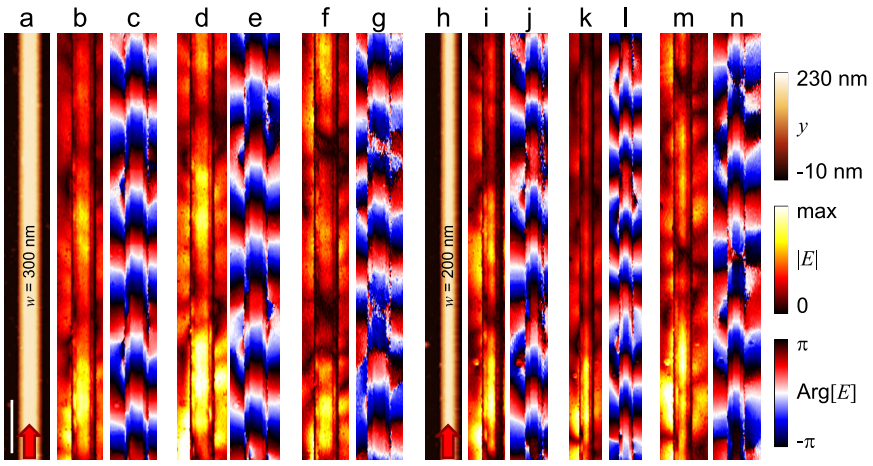

Fig. 4. Pseudocolor SNOM images of (a, h) topography y and (b-g, i-n) near-field amplitude and phase for waveguide width of (a-g) 300 and (h-n) 200 nm, recorded at the illumination wavelength of: (b, c, i, j) 1425, (d, e, k, l) 1525, and (f, g, m, n) 1625 nm, respectively. The propagation direction is illustrated with red arrow in (a, h). Scale bar in (a) represents 1 μm.

profile of the first mode shows strong field just outside the ridge, which agrees well with the simulated mode profile [Fig. 1(c)].

3.5. *Experimental results*

The effective mode index and propagation length, extracted by fitting all SNOM maps, are presented in Fig. 6, and compared with numerical simulations. As expected, the effective mode index decreases and propagation length increases, when the wavelength increases. The influence of the waveguide width w is not so straightforward: according to simulations, its decrease from 300 to 200 nm should lower the effective mode index, which will result in weaker mode confinement and, correspondingly, longer propagation length. The experimental results show the same trend for the effective mode index, but the propagation length became longer for the w = 200 nm. This disagreement can be explained by different waveguide geometry in the experiment, compared to the design (for example, it was mentioned above about the tendency of gold to form a meniscus with silica ridge walls). Also, it does not contradict the fundamental trade-off between the mode confinement and propagation length since mode confinement is not straightforwardly related to the effective mode index. For example, such decrease in both effective mode index and propagation length for the same change of the width was observed in simulations for any ridge height in the range 130-170 nm. Another reason for shorter propagation length in the experiment is the higher Ohmic losses in the metal due to the Ti adhesion layer.

4. Conclusion

We designed, fabricated and investigated a novel hybrid plasmonic waveguide, formed by a dielectric ridge on a dielectric substrate, coated with a noble metal. Such waveguide supports the propagation of a bound plasmonic mode with a subwavelength confinement (within the ridge of 300 nm in width and 200 nm in height) and moderate losses (propagation length ~10 μm) at telecommunication wavelength range (1425-1625 nm). The waveguiding was demonstrated experimentally, and the main mode characteristics (effective mode index, propagation length and mode profile) were determined both from numerical simulations and from the amplitude- and

Optics EXPRESS

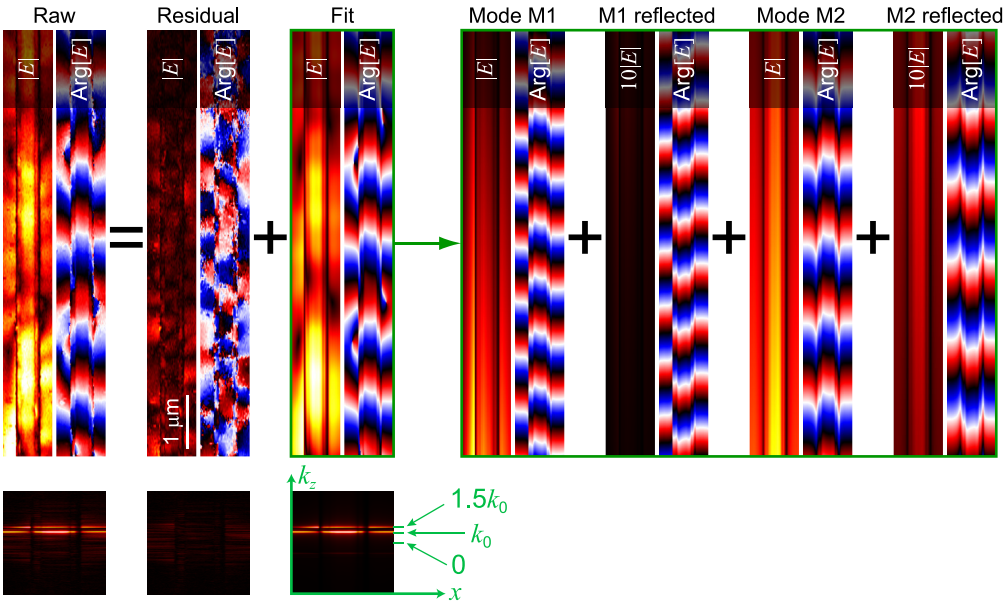

Fig. 5. Results of fitting procedure for $\lambda = 1525$ nm and $w = 300$ nm. The near-filed distribution was fitted with two modes. The amplitude $|E|$ of reflected modes was 10 times enhanced for visibility. Bottom row: amplitude after one-dimensional FT along z-axis, corresponding to the above raw, residual and fitted near-field maps.

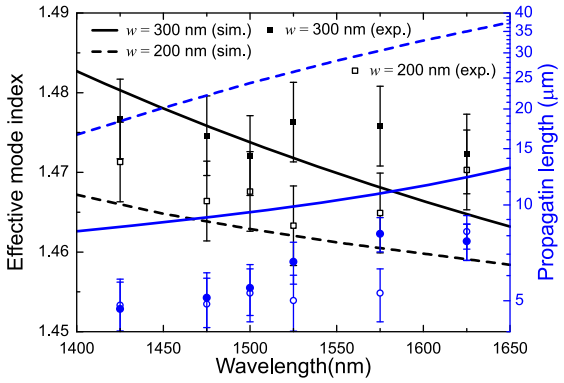

Fig. 6. Dispersion properties of the mode, expressed in terms of the effective mode index (black squares and lines) and propagation length (blue circles and lines) as a function of the wavelength. The experimental results are shown with points and compared to the simulation results for the waveguide width of 300 nm (solid lines and points) and 200 nm (dashed lines and hollow squares/circles). The error bars were estimated from measurements of different duplicates and different excitation directions (when the coupling was done at another end of the same waveguide).

Optics EXPRESS

phase-resolved near-field images. Such waveguides feature a simple design, with the potential to be fabricated with a template stripping technique [8, 10] or nanoimprint lithography [19, 20], enabling mass production and large scale integration in quantum plasmonics circuits. The possibility of strongly influencing the mode properties can further be exploited in mode shaping and sensing applications.

Funding

European Research Council (ERC), Grant 341054 (PLAQNAP), NSF MRSEC DMR-1120923; Air Force Office of Scientific Research (AFOSR) Grant FA9550-14-1-0138; Air Force Office of Scientific Research (AFOSR) MURI grant (FA9550-14-1-0389).

Acknowledgments

The authors thank Kasper Haxholm Filtenborg for recording SNOM scans.

128.46.222.102 {ts '2017-05-24 10:58:30'}